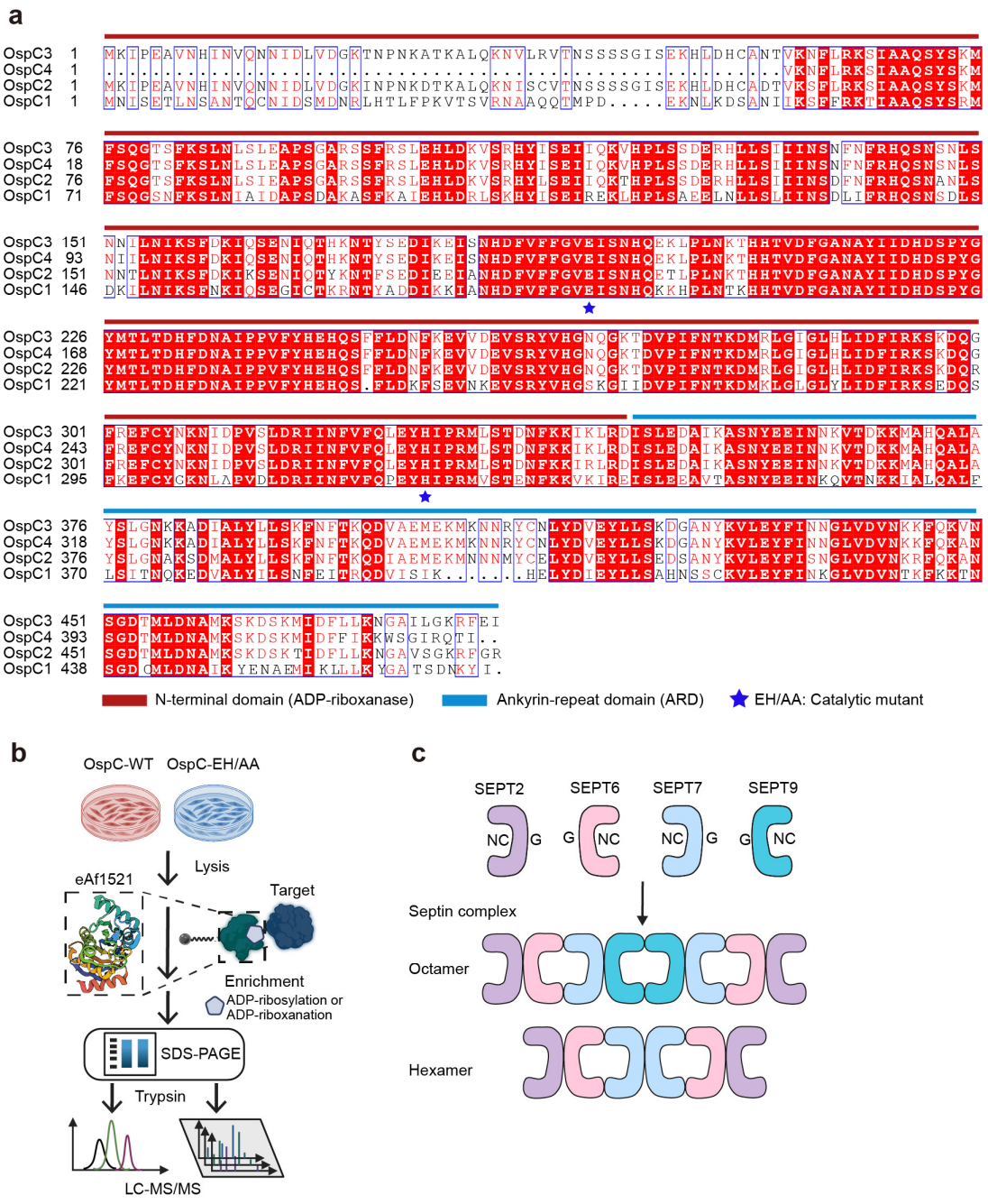

Fig. S1. A proteomic screen identified septins as conserved substrates of OspC family effectors.

(a) Multiple sequence alignment of OspC effectors. The alignment was performed using the ClustalW2 algorithm and visualized with ESPript 3.0 (http://espript.ibcp.fr/ESPript/cgi-bin/ESPript.cgi). Identical residues are highlighted in red, while conserved residues are shown in red text. The N-terminal ADP-riboxanase domain (N domain) and the C-terminal ankyrin-repeat domain (ARD) are annotated along the sequences. The mutated residues of enzymatic activity-deficient mutants (EH/AA) are marked with blue pentagrams right below.

(b) A schematic diagram of the ADP-ribosylome profiling strategy. To identify the potential substrates of OspC proteins, we analyzed the ADP-ribosyolome of 293T cells transfected with

OspC1 or OspC3 (while the catalytically dead mutants were used as controls). The enrichment of potentially ADP-riboxanated and ADP-ribosylated cellular proteins was achieved with the use of engineered Af1521 (eAf1521), a macrodomain-containing protein that has high affinity towards ADP-ribose. Protein ratios were calculated as protein spectral counts in WT OspC1 or OspC3 samples divided by those in their EH/AA mutant samples. Proteins with Log_2Ratio (WT vs. EH/AA) > 3 were considered as candidate substrates.

(c) A schematic representation of organization of septin-septin oligomers with septins from different groups shown in distinct colors. Septins interact with adjacent subunits through alternating G-interfaces and NC-interfaces. Each septin group member is present in two copies which are symmetrically arranged within the complex.

1b: Created in BioRender. Zhang, Y. (2025) https://BioRender.com/yi2pswg

1c: Created in BioRender. Zhang, Y. (2025) https://BioRender.com/764had3

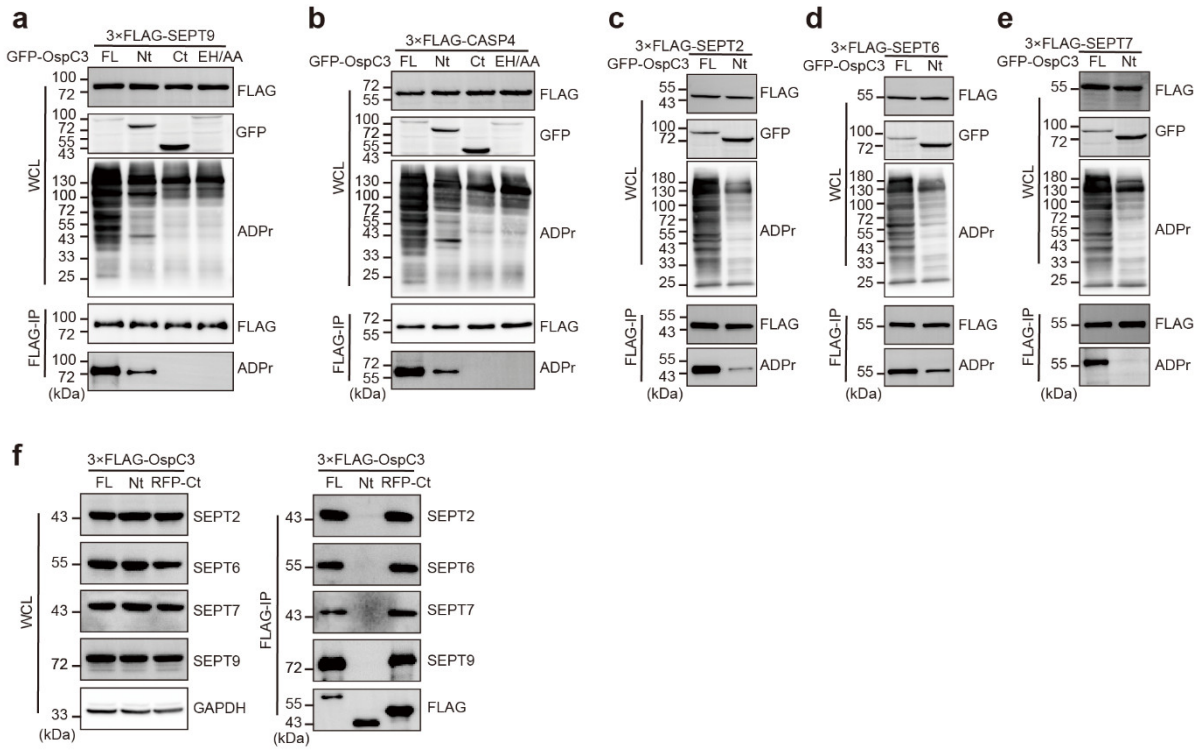

Fig. S2. The C-terminal ARD domain of OspC3 mediates its interaction with septins.

(a, b) OspC3 ADP-riboxanated SEPT9 and CASP4 in a manner dependent on both its enzymatic activity and ARD. **(a)** 293T cells were co-transfected with FLAG-SEPT9 and GFP-OspC3 or its variants, lysed, and immunoprecipitated using a FLAG antibody. **(b)** FLAG-CASP4 samples were prepared following the same procedure. The immunopurified samples were blotted with indicated antibodies. FL, Nt, and Ct represent full-length, N-terminal, and C-terminal regions of OspC3, respectively.

(c–e) OspC3 modified SEPT2, SEPT6, and SEPT7 dependent on its C-terminal ARD. The samples were prepared as described above and analyzed by Western blotting using indicated antibodies. FL and Nt represented full-length and N-terminal regions of OspC3 respectively.

(f) OspC3 interacted with septins via its C-terminal ARD. FLAG-OspC3 or its truncation mutants were immunoprecipitated from 293T cells using a FLAG antibody, and analyzed by immunoblotting to assess the interactions with indicated septin subunits. FL, Nt, and Ct represent full-length, N-terminal, and C-terminal regions of OspC3, respectively.

For **a–f**, experiments were repeated three times with similar results.

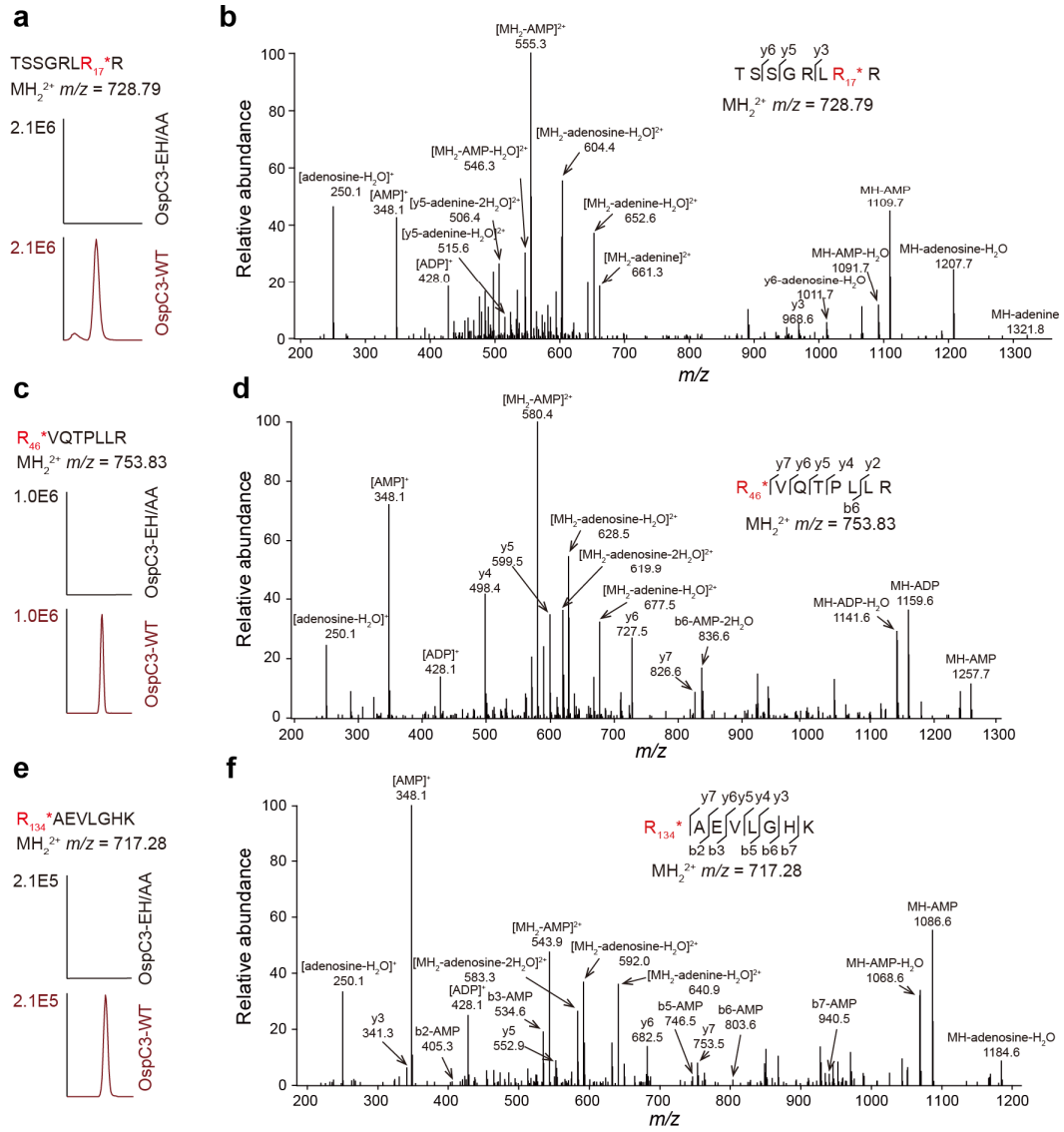

Fig. S3. LC-MS/MS analyses of modification sites of SEPT9.

(a, c, and e) FLAG-SEPT9 was co-expressed with either WT OspC3 or the enzymatically inactive EH/AA mutant in 293T cells. Immunoprecipitated samples were fractionated by SDS-PAGE and analyzed by LC-MS. Extracted ion chromatograms of ADP-riboxanated SEPT9 peptides containing Arg17 **(a)**, Arg46 **(c)** or Arg134 **(e)**.

(b, d, and f) MS/MS spectra of ADP-riboxanated SEPT9 peptides containing Arg17 **(b)**, Arg46 **(d)** or Arg134 **(f)**. The observed b and y fragment ions are annotated along the peptide sequence displayed above each spectrum.

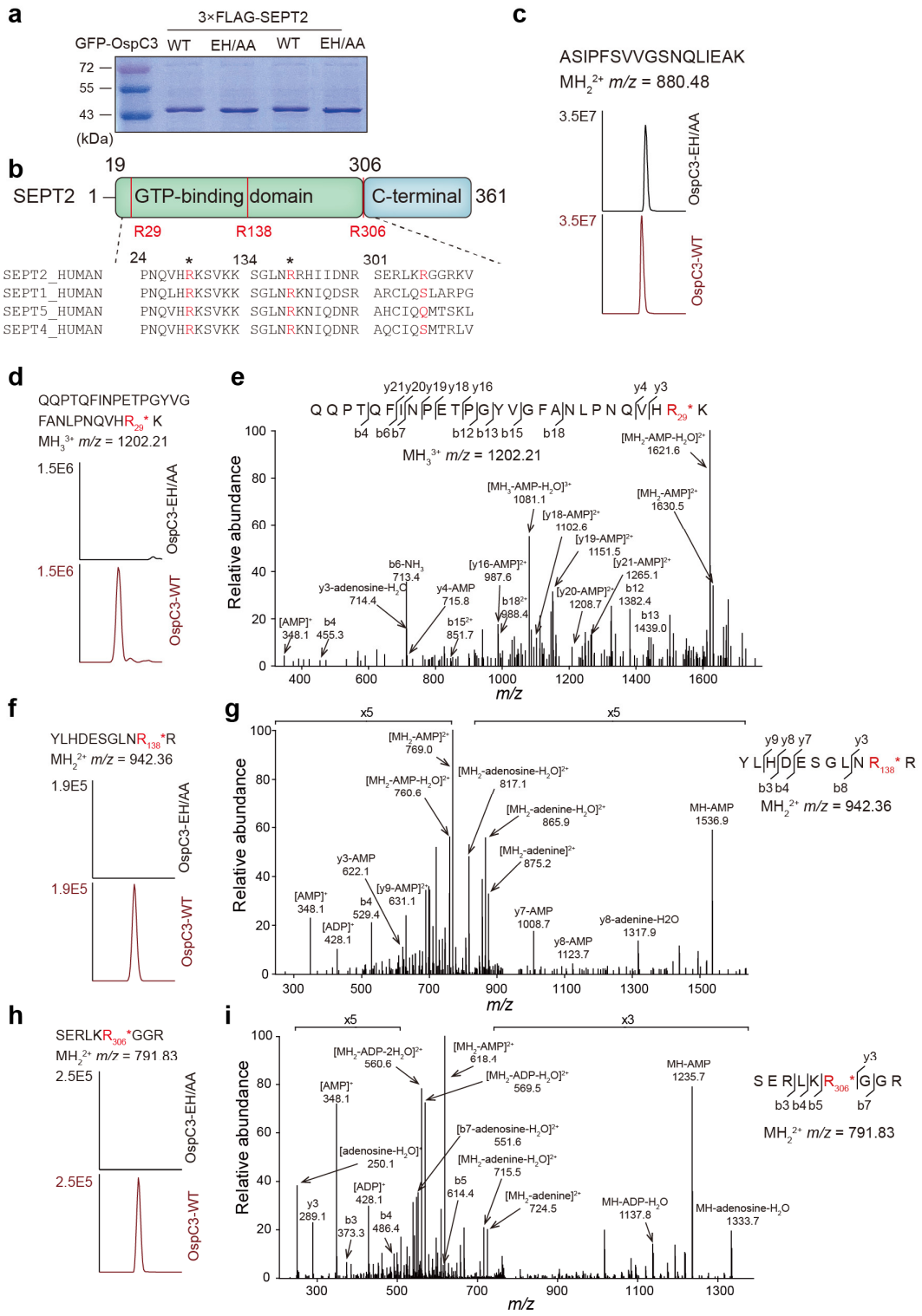

Fig. S4. LC-MS/MS analyses of modification sites of SEPT2.

(a) Coomassie blue-stained FLAG-SEPT2 samples that were immunoprecipitated from 293T cells co-transfected with GFP-OspC3-WT or GFP-OspC3-EH/AA.

(b) Identified ADP-riboxanation sites of SEPT2. Multiple sequence alignment was performed for the members of the SEPT2 subgroup using the ClustalW2 algorithm. ADP-riboxanation

sites are highlighted in red, and asterisks indicate conserved residues.
(c) Extracted ion chromatograms of an unmodified control peptide from SEPT2.
(d, f, and h) Extracted ion chromatograms of ADP-riboxanated SEPT2 peptides containing Arg29 **(d)**, Arg138 **(f)** or Arg306 **(h)**.
(e, g, and i) MS/MS spectra of ADP-riboxanated SEPT2 peptides containing Arg29 **(e)**, Arg138 **(g)** or Arg306 **(i)**. The observed b and y fragment ions are annotated along the peptide sequence displayed above each spectrum.

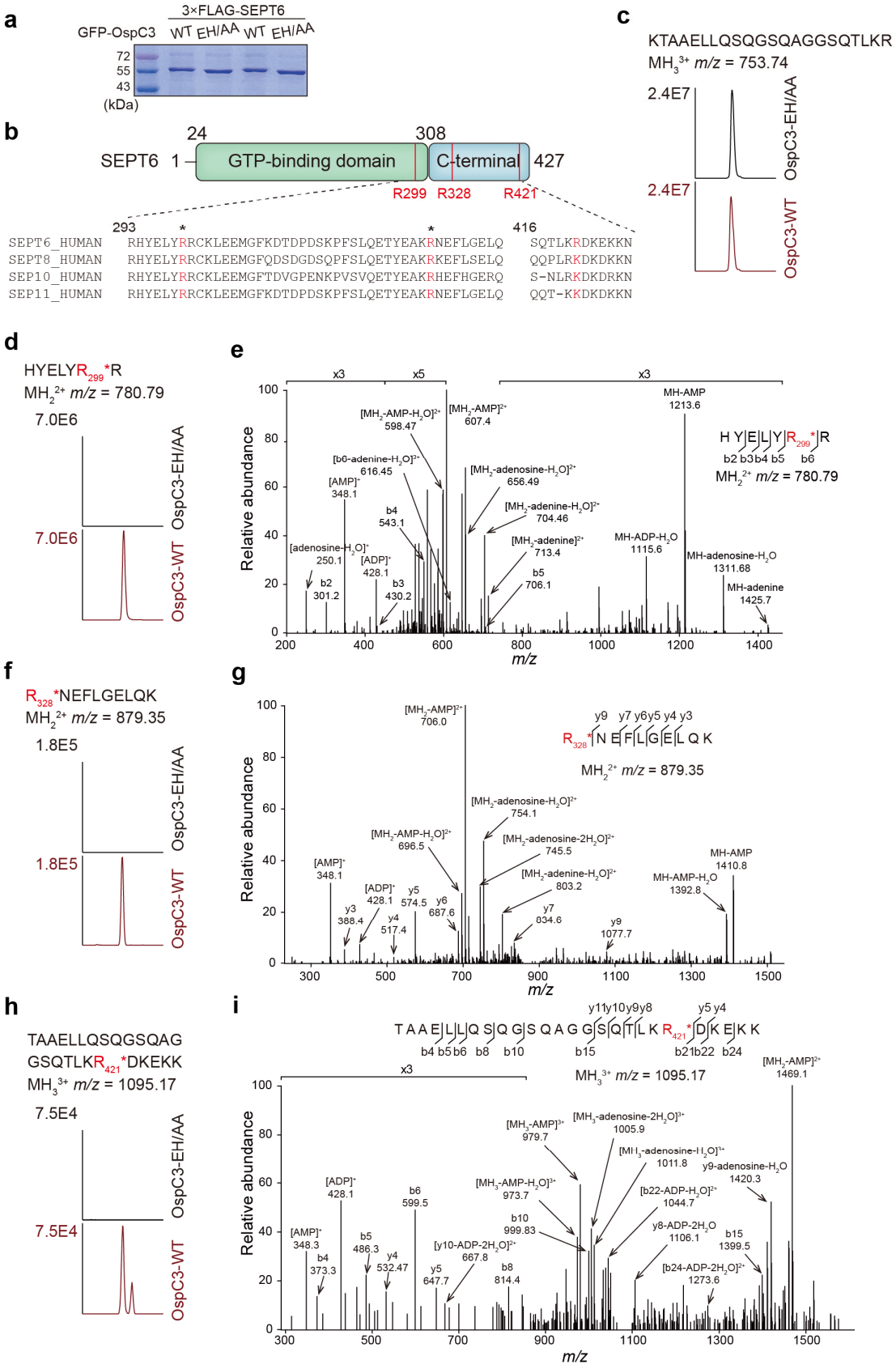

Fig. S5. LC-MS/MS analyses of modification sites of SEPT6.

(a) Coomassie blue-stained FLAG-SEPT6 samples that were immunoprecipitated from 293T cells co-transfected with GFP-OspC3-WT or GFP-OspC3-EH/AA.
(b) Identified ADP-riboxanation sites of SEPT6. Multiple sequence alignment was performed for the members of the SEPT6 subgroup using the ClustalW2 algorithm. ADP-riboxanation sites are highlighted in red, and asterisks indicate conserved residues.
(c) Extracted ion chromatograms of an unmodified control peptide from SEPT6.
(d, f, and h) Extracted ion chromatograms of ADP-riboxanated SEPT6 peptides containing Arg299 **(d)**, Arg328 **(f)** or Arg421 **(h)**.
(e, g, and i) MS/MS spectra of ADP-riboxanated SEPT6 peptides containing Arg299 **(e)**, Arg328 **(g)** or Arg421 **(i)**. The observed b and y fragment ions are annotated along the peptide sequence displayed above each spectrum.

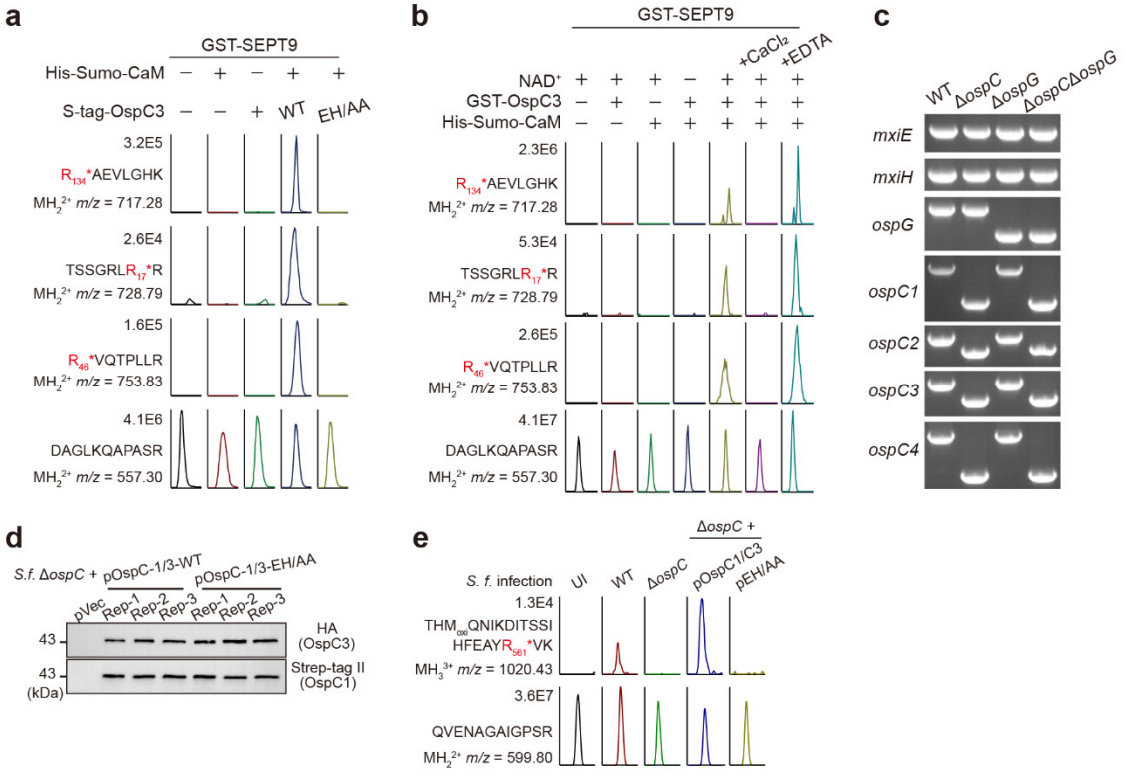

Fig. S6. OspCs directly ADP-riboxanate SEPT9 *in vitro* and during bacterial infection.

(a) LC-MS analysis of SEPT9 samples co-expressed with CaM and OspC3 in *E. coli*. Extracted ion chromatograms of an unmodified control peptide (DAGLKQAPASR, *m/z* = 557.30) and ADP-riboxanated peptides containing Arg17 (*m/z* = 728.79), Arg46 (*m/z* = 753.83), and Arg134 (*m/z* = 717.28). Notably, modified peptides containing Arg561 were not detected under these conditions.

(b) LC-MS analysis of SEPT9 samples from *in vitro* biochemical reactions. Extracted ion chromatograms of an unmodified control peptide (DAGLKQAPASR, *m/z* = 557.30) and ADP-riboxanated peptides containing Arg17 (*m/z* = 728.79), Arg46 (*m/z* = 753.83), and Arg134 (*m/z* = 717.28). Notably, modified peptides containing Arg561 were not detected under these conditions.

(c) PCR-based genotyping of *S. flexneri* WT and knockout strains. Genomic DNA from WT, Δ*ospC*, Δ*ospG*, and Δ*ospC*Δ*ospG* strains were amplified using gene-specific primers targeting *mxiE*, *mxiH*, *ospG*, *ospC1*, *ospC2*, and *ospC3*. The DNA fragments corresponding to the knockout strains (Δ*ospC*, Δ*ospG*, and Δ*ospC*Δ*ospG*) are smaller in size compared to the WT due to the removal of specific gene regions.

(d) Western blots confirmed the expression of OspC effectors in complemented *S. flexneri* Δ*ospC* strains. Bacterial strains carrying the empty vector (pVec), pOspC-1/3-WT, or pOspC-1/3-EH/AA were analyzed. Three independent biological replicates (Rep-1, Rep-2, and Rep-3) were included for each condition. HA-tagged OspC3 and Strep-II-tagged OspC1 were detected using specific antibodies.

(e) LC-MS analysis of endogenous SEPT9 from infected HeLa cells. The same samples shown

in Fig. 2j were separated by SDS-PAGE prior to LC-MS analysis. Extracted ion chromatograms of an unmodified control peptide (m/z = 599.80) and an Arg561-containing ADP-riboxanated peptide (m/z = 1020.43) are shown.

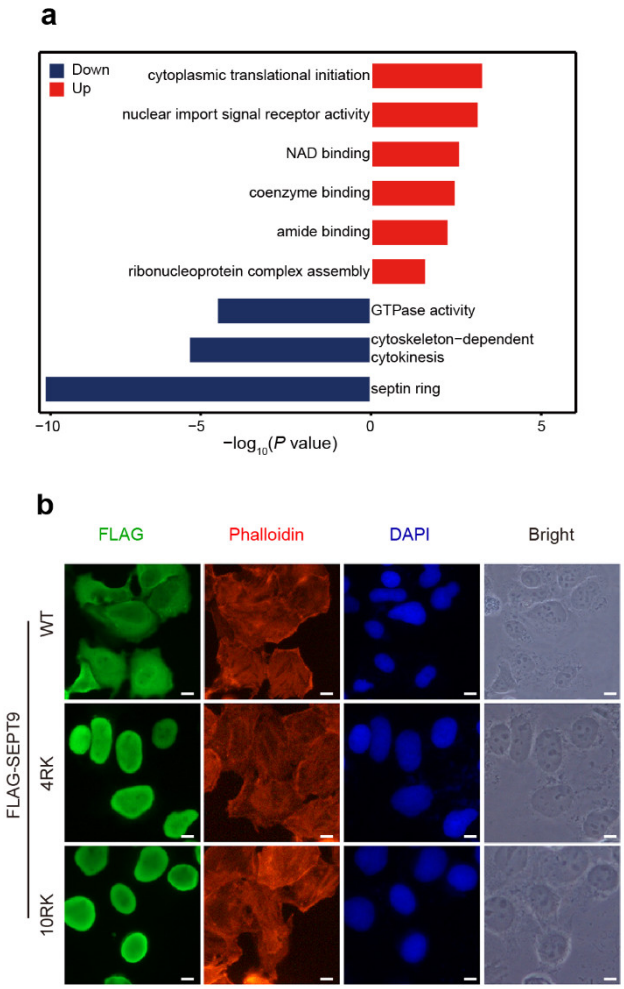

Fig. S7. OspC-mediated ADP-riboxanation destabilizes the septin complex, related to Figure 3.

(a) GO analysis of SEPT9-associated proteins upon ADP-riboxanation. Enriched terms (i.e., proteins with increased interactions) are shown in red, whereas those underrepresented ones (i.e., proteins with impaired SEPT9 association upon modification) are shown in blue. *P* values were calculated using a one-sided hypergeometric test implemented in the R package clusterProfiler, without multiple testing correction.

(b) Mutations of SEPT9 ADP-riboxanation sites disrupt its subcellular localization, leading to increased nuclear distribution. HeLa cells were transfected with either WT SEPT9 or its mutant constructs and analyzed by immunofluorescence. Representative images from two independent experiments are shown. Scale bar, 10 μm.

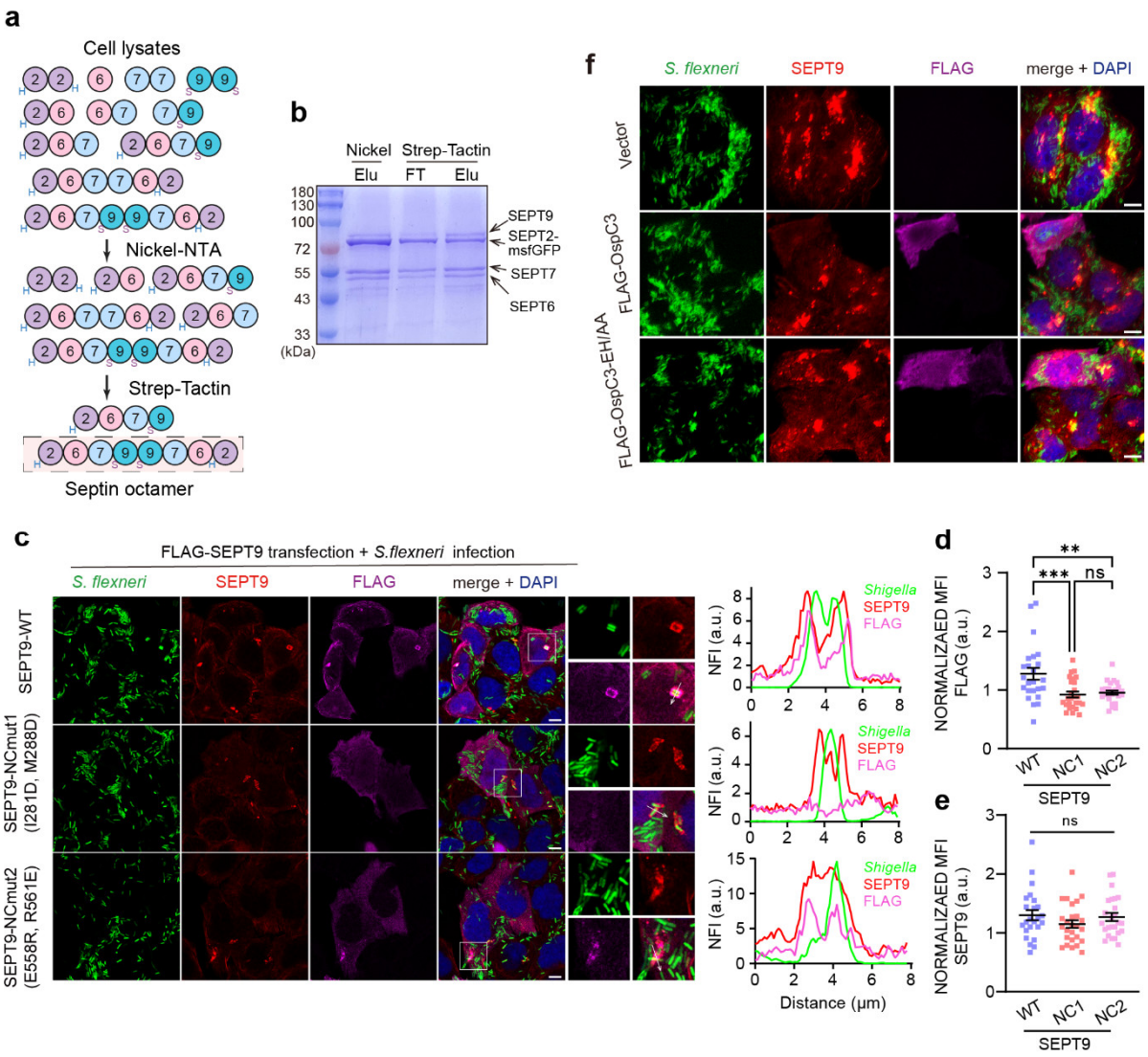

Fig. S8. ADP-riboxanation of SEPT9 Arg561 destabilizes septin octamers and obstructs septin cage assembly.

(a) Schematic representation of a two-step purification strategy for preparing SEPT9-containing stoichiometric octamers. The first step involves Ni-NTA affinity purification to isolate His-tagged septins, followed by Strep-Tactin affinity purification to enrich the stoichiometric complex. Details are provided in the Methods section.

(b) SDS-PAGE analysis of purified septin octamers. Lanes from left to right are eluates from Ni-NTA purification, flow-through (FT) and eluates from Strep-Tactin purification. The final eluates (Elu) from Strep-Tactin purification show stoichiometric protein bands corresponding to SEPT9, SEPT2-msfGFP, SEPT7, and SEPT6.

(c–e) The NC-interface of SEPT9 is important for its incorporation into septin cages. Sample preparation and data analysis were described in Fig. 5a–c. Representative images (scale bar, 10 μm) from $n = 3$ independent experiments are shown in **(c)**. Normalized fluorescence intensity (NFI) profiles were plotted along the arrows in the merged images. Normalized mean fluorescence intensity (MFI) of *Shigella*-associated FLAG-SEPT9 **(d)** and total SEPT9 **(e)** are

presented as mean ± SEM from $n = 25$ fields of view. Statistical analysis was performed using one-way ANOVA followed by Tukey's multiple comparisons test (two-sided).
(f) Ectopic expression of OspC3 potently inhibits the assembly of septin cages in an enzymatic activity-dependent manner. HeLa cells were transfected with FLAG-OspC3 or its controls for 20 h, followed by infection with *S. flexneri* (MOI = 30) for 2 h and 40 min. Cells were then analyzed by immunofluorescence using indicated antibodies. Representative confocal maximum intensity projection images from Z-stacks (scale bar, 10 μm), derived from $n = 3$ independent experiments, are shown.